Editors' Suggestion | Featured in Physics

Oxygen Opacity Measurements at High-Energy-Density Conditions

J. E. Bailey,[1,*] D. C. Mayes,[2] G. P. Loisel,[1] T. Nagayama,[1] D. Aberg,[3] C. Blancard,[4,5] J. Colgan,[6] Ph. Cossé,[4,5] G. S. Dunham,[1] G. Faussurier,[4,5] C. J. Fontes,[6] F. Gilleron,[4,5] I. Golovkin,[7] T. A. Gomez,[8] M. F. Gu,[7] S. B. Hansen,[1] H. Huang,[9] C. A. Iglesias,[3] C. Monton,[9] J.-C. Pain,[4,5] R. Santana,[9] and B. W. Wilson[3]

[1]*Sandia National Laboratories, Albuquerque, New Mexico 87185, USA*
[2]*University of Texas, Austin, Texas, USA*
[3]*Lawrence Livermore National Laboratory, Livermore, California 94550, USA*
[4]*CEA, DAM, DIF, F-91297 Arpajon, France*
[5]*Université Paris-Saclay, CEA, LMCE, F-91680 Bruyères-le-Châtel, France*
[6]*Los Alamos National Laboratory, Los Alamos, New Mexico 87545, USA*
[7]*Prism Computational Science, Madison, Wisconsin, USA*
[8]*University of Colorado, Boulder, Colorado, USA*
[9]*General Atomics, San Diego, California 92186-5608, USA*

(Received 22 July 2025; accepted 25 September 2025; published 12 November 2025)

We present the first benchmark measurements of oxygen opacity at high-energy-density, crucial for understanding stellar interiors. A 3–5-μm thick SiO_2 sample was heated using a Z facility x-ray source, and opacity was measured in the 5–19.5 Å range with multiple spectrometers. The electron temperature and density inferred from Si *K*-shell spectra were 148 ± 4 eV and $8.6 \pm 1.4 \times 10^{21}$ cm^{-3}, respectively. Six experiments showed opacity reproducibility within ±15% and 5%–25% opacity uncertainty. Measured oxygen opacity and seven different opacity models exhibit extraordinary overall agreement. Discrepancies near the H-like photon ionization threshold and in certain spectral lines suggest the need for model refinements.

DOI: 10.1103/n2k6-358d

Energy generated by nuclear fusion in stars like the Sun is transported through the interior by x-ray radiation. The structure and evolution of these stars depend on *opacity*, the property of matter that controls photon absorption. The opacity depends on the star's elemental composition and the wavelength dependent absorption each element contributes. A revision of solar abundances [1] led to a discrepancy between the predicted solar interior structure and helioseismic observations, known as the "solar problem" [2–4]. Abundances are still debated ([4], and references therein), but the solar problem could largely be resolved if the actual opacity is higher than models predict.

Photon absorption involving bound electrons dominates radiative energy transport in the Sun. Solar opacity is especially sensitive to iron and oxygen because these are abundant elements that retain bound electrons at solar interior temperatures [Fig. 1(a)]. Neon is another element that makes a notable contribution to solar opacity and merits future studies. The challenges for understanding iron and oxygen opacity in stars are different. Iron near the solar radiation–convection zone boundary (CZB) retains 6–10 bound electrons. Difficulties include modeling about 1×10^9 bound-bound transitions, line broadening for many-electron ions, multiply excited states, complex satellite transitions, and proposed (but controversial) mechanisms [5–9]. On the other hand, oxygen retains 0–2 bound electrons, resulting in simpler atomic structure. Unlike iron, oxygen opacity is very sensitive to ionization balance because bound-free and bound-bound opacities vanish for bare ions but are finite for H-like or He-like ions. The ionization and thus, the opacity, depends on continuum lowering [10–13], an incompletely understood process describing how atomic bound levels are delocalized in dense plasma and become part of the continuum.

Benchmark iron opacity measurements at conditions similar to the solar radiation–convection zone boundary found higher-than-predicted iron opacity [19]. Those results solve about half the solar problem, but they remain controversial due to unresolved differences between opacity predictions and the data. The discussion above implies that benchmark oxygen opacity measurements are essential regardless of the eventual resolution of the iron opacity discrepancies.

*Contact author: jebaile@sandia.gov

Published by the American Physical Society under the terms of the Creative Commons Attribution 4.0 International license. Further distribution of this work must maintain attribution to the author(s) and the published article's title, journal citation, and DOI.

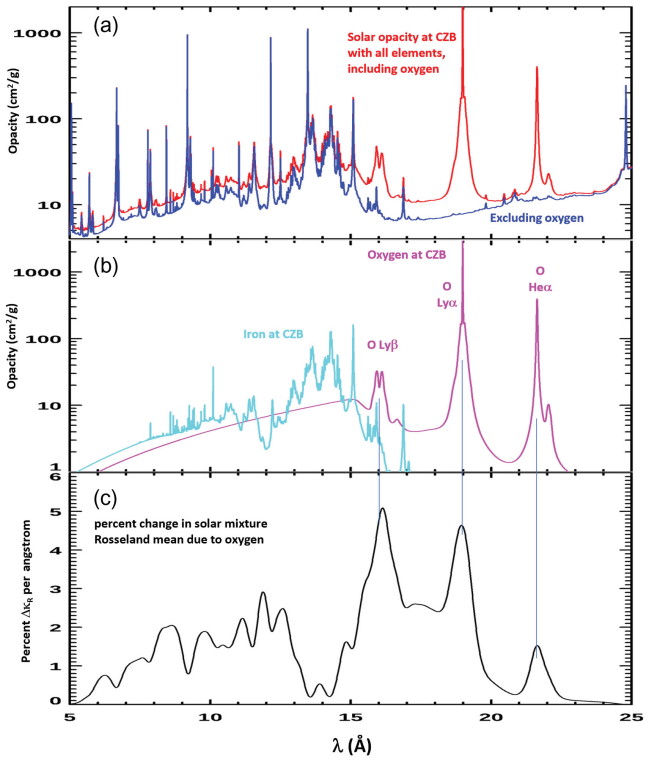


FIG. 1. Calculations with the OP opacity model [14–16] near solar convection zone base (CZB) conditions ($T_e \sim 193$ eV,$n_e = 1 \times 10^{23}$ cm^{-3}) show oxygen contributes notably to the total solar matter opacity (a). The red curve is total opacity for 17 elements using Ref. [17] composition and the blue curve excludes oxygen. Oxygen H-like and He-like bound-bound features and bound-free continuum contribute opacity (b). The importance of specific oxygen features for the solar Rosseland mean opacity [18] is quantified by calculating the percent mean opacity change per unit wavelength (c).

In this Letter we report the first oxygen opacity benchmark measurements at high-energy-density (HED) conditions: electron temperature $T_e \sim 148 \pm 4$ eV and electron density $n_e \sim 8.6 \pm 1.4 \times 10^{21}$ cm^{-3}. This advance required novel opacity sample fabrication and refined spectrometers to measure x-ray transmission over a 5–19.5 Å range. The T_e and n_e values produce the charge states that exist in stellar interiors and the wavelength range measures the key bound-bound and bound-free oxygen transitions. The density and temperature were roughly 10× and 1.3× lower than at the solar CZB [$T_e \sim 187$ eV; $n_e \sim 9 \times 10^{22}$ cm^{-3} ([2,3], and references therein)]. Definitive solar oxygen opacity conclusions await future results at higher density and temperature, especially considering the unexpected opacity trends for the iron group elements [19–21]. Nevertheless, the present research provides important outcomes: (1) the overall agreement between model predictions and the data is consistent with accurate model approximations and accurate experimental methods, establishing a foundation for research at more extreme conditions and (2) for the first time, physics approximations used by opacity models to describe ionization, continuum lowering, bound-free, and bound-bound transitions can be tested for oxygen at HED conditions.

Radiation transport models in stars depend on the Rosseland mean opacity [18], a harmonic average weighted by the temperature derivative of the Planck function. The solar interior Rosseland mean is typically approximated by summing contributions from the 17 most abundant elements [22]. A comparison of solar opacity calculations [14–16] with and without oxygen highlights oxygen's significance [Fig. 1(a)]. But which oxygen absorption features contribute the most to the solar Rosseland mean [Fig. 1(b)]? Calculating the percent change in the solar Rosseland mean per unit wavelength due to oxygen shows that the oxygen bound-free, the H-like line strengths and widths, and the absorption between the Ly α and Ly β lines have the biggest impact [Fig. 1(c); see End Matter]. This procedure determines which opacity features require the most scrutiny. A simple comparison of the Rosseland weighting function spectrum with the individual element opacity spectrum alone is inadequate.

A goal for oxygen opacity measurements is model tests for bound-free and spectral line absorption. Investigating plasma density effects, including continuum lowering and the delocalization of bound levels into the continuum, is important since it affects the number of bound electrons available to contribute absorption. This can be accomplished by examining the opacity spectrum near the photon ionization threshold. A complication is that continuum lowering, bound level merging with continuum states, and line broadening are intertwined (e.g., see Ref. [10]).

Key requirements for oxygen opacity benchmark experiments include samples heated enough to produce the relevant charge states, wavelength-dependent opacity measurements in the 7–20 Å range that spans the relevant transitions, accurately quantified uncertainties, and demonstrated reproducibility. Other critical requirements [23,24] include independent plasma diagnostics, minimal (measured) backgrounds, and plasma uniformity.

To our knowledge there are no previous oxygen x-ray opacity experiments that meet these requirements. Ongoing oxygen experiments at the National Ignition Facility (NIF) laser have provided preliminary data [25], but uncertainty and reproducibility evaluations remain in progress and oxygen transmission-opacity results were not deemed conclusive. These efforts rest on a foundation provided by nearly 40 years of opacity measurements. The methods were elucidated first in laser-driven experiments (see Ref. [23]) and subsequently adapted to experiments at Z [19–21,26–29], where the increased drive energy and novel experiment designs enabled the first opacity measurements at stellar interior temperatures.

The present experiments used the Z opacity science platform [19–21,26–29] (Supplemental Material, Fig. 1;

see Ref. [30]). Dynamic hohlraum x-rays heat a thin SiO_2 sample tamped with CH. The heating x-rays from the 200–400 eV quasi-Planckian source stream through the sample, promoting uniformity. A bright x-ray burst upon stagnation provides a ∼3 nsec duration backlight viewed through the sample by six space-resolving convex-crystal spectrometers. This measures the x-ray transmission. The sample conditions are inferred by analyzing the Si K-shell spectral absorption in the 5–7 Å range. Oxygen opacity is inferred in the 7–19.5 Å range. Multiple opacity measurements in each experiment and performing six independent experiments with different sample thicknesses fosters accuracy and the ability to quantify uncertainties.

Oxygen has relatively low opacity per atom because each atom only has 0, 1, or 2 bound electrons for the conditions explored here. The SiO_2 samples used $1.5–2.5 \times 10^{19}$ oxygen atoms/cm^2 to optimize the oxygen bound-free, windows between lines, and line wing measurements. Sample areal density was inferred from the measured Si He δ and He ε line optical depths and preshot x-ray transmission [31]. Agreement between the two methods is evidence for accuracy (Supplemental Material [30]), but characterizing these samples is novel and systematic errors that might shift the entire experimental opacity spectrum up or down (by perhaps 10%) cannot be precluded.

These experiments used either 4 or 6 independent space-resolved convex-crystal spectrometers arranged at various angles with respect to the z-pinch axis (Supplemental Material [30]). Extending the wavelength range to cover 5–19.5 Å was a key innovation. This span is unprecedented in opacity research but required here to simultaneously record diagnostic lines from K-shell Si and the most important oxygen spectrum features. The difficulties of making measurements at long wavelengths were surmounted by using rubidium acid phthalate (RAP) crystals that suppress second order x-rays at wavelengths above ∼13.65 Å and a thin 0.2 μm polyimide +0.2 μm Al light tight filter that transmits ∼60% at 20 Å. An extensive set of baffles protects the filters from debris.

The transmission determination relies on twenty-seven calibration experiments that recorded more than 100 spectra without any opacity sample. Each calibration can be treated as an opacity measurement with known transmission and consequently verify the quantitative accuracy. A preliminary version of this method was deployed in [21] and a complete description is in preparation. The information contained in the transmission spectra includes the oxygen bound-bound and bound-free absorption and the diagnostic lines (see End Matter, Fig. 4). The Si K-shell spectroscopic diagnostic procedure is very similar to the sequential line analysis methods employed to infer plasma conditions from Mg K-shell spectra in iron opacity experiments [27,32]. The average values and their standard deviations were $T_e = 148 \pm 4$ eV and

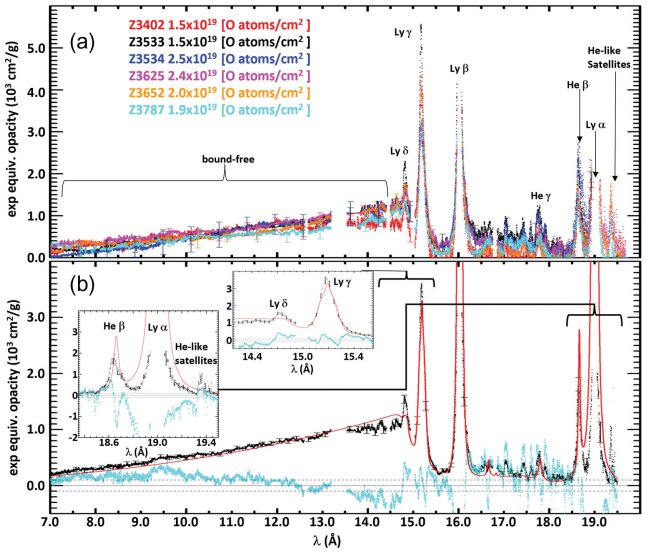


FIG. 2. Oxygen experiment-equivalent opacity (see End Matter) measured on six experiments at the Z facility (a), demonstrating reproducibility within the 1σ uncertainties. Panel (b) displays the weighted average from these six experiments (black dots with error bars) compared with OP model predictions (red) at $T_e = 152$ eV and $n_e = 1.0 \times 10^{22}$ cm^{-3}. The cyan curve is residual = [(data–model)/uncertainty], multiplied by 100 to place it on the same scale as the opacity. Horizontal dashed lines represent residual difference = 1σ. The insets are enlarged views of the oxygen Ly δ-Ly γ and He β-Ly α-He-like satellite regions.

$n_e = 8.6 \pm 1.4 \times 10^{21}$ cm^{-3} for the six experiments described here. The temperature and density from the six experiments agreed with the average values within the ±3% and ±20% uncertainties in the temperature and density values, respectively.

The oxygen opacity is inferred from each experiment by taking the natural log of transmission and dividing by the oxygen areal density. The six experiments generally agreed within the $\pm 5\% - 25\%$ uncertainty in the individual experiment opacity [Fig. 2(a)]. Each experimental opacity has uncertainty that includes the transmission uncertainty, the ±30% background uncertainty [33], and ±4% areal density uncertainty.

The oxygen opacity measured in the 7–14 Å region spanning the bound-free absorption is within 1σ of the average opacity for 5 out of 6 experiments. A single experiment differs by 1.2σ. Therefore, the experiment variability is consistent with the uncertainties determined in each experiment and a weighted average is an appropriate representation of the measured value [Fig. 2(b)]. Furthermore, using an average opacity is valid because there is no statistically significant difference in the plasma conditions between the six experiments. The uncertainty in the weighted-average opacity is approximately ±8% over the 7–14 Å range. The uncertainty elsewhere is higher. In addition, the data are not displayed in the Lyβ and Lyα line

cores (defined here as transmission less than 0.1) because those lines have high optical depth at line center.

The plasma is most likely uniform because it is relatively transparent to the bulk of the 300–1200 eV heating x-ray spectrum. Past experimental spatial and temporal uniformity measurements support this assertion [27,34,35]. The oxygen areal densities ranged from $1.5–2.5 \times 10^{19}$ O atoms/cm^2. The agreement between experiments verifies that the data satisfy the Beer-Lambert-Bouguer Law and ameliorates concerns over possible systematic errors [23,24].

The overall agreement between the predictions and measured weighted average (taken over the six experiments, as described above) oxygen opacity is outstanding [see Figs. 2(b), 3, and 6], especially considering that no previous HED oxygen experiments were available. Although several important discrepancies are discussed below, these do not negate the reassuring general agreement. The comparison is with seven different opacity models: OP [14–16], ATOMIC [36], OPAS [37], TOPAZ [38], SCO-RCG [39], SCRAM [40], and PrismSPECT [41]. The OP model used here is the open-access online version generously made available by the OP team [16]. Refined versions of OP are under development [42,43], but the online version has been extensively used for stellar astrophysics (e.g., [44]). Another method that may provide additional insight as it is further developed is described in [45].

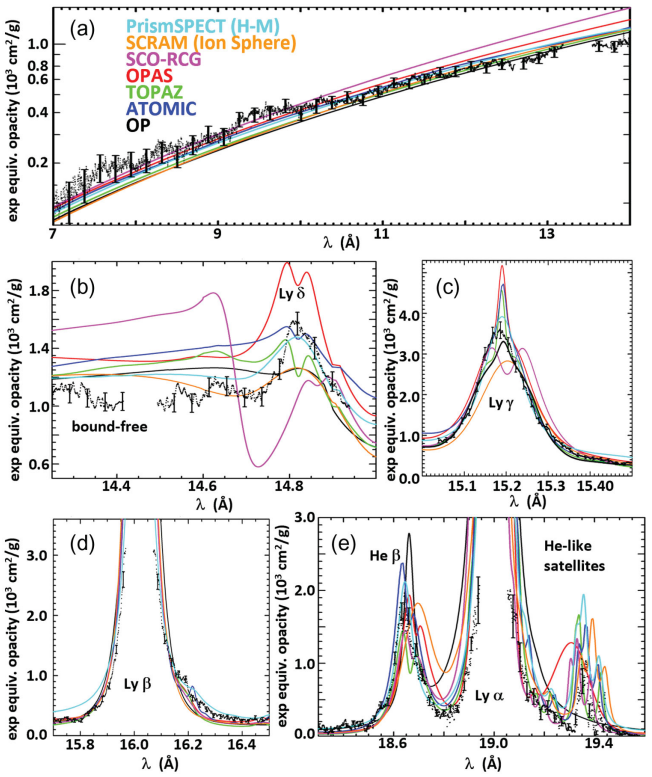


FIG. 3. Oxygen weighted-average experiment-equivalent opacity from six Z experiments (black dots with 1σ error bars) compared to seven different model calculations (colors). PrismSPECT used the Hummer-Mihalas and SCRAM used the Ion Sphere IPD approximations, respectively [10,40,41]. All other models used their default IPD method. All models except OP are at $T_e = 148$ eV and $n_e = 8.6 \times 10^{21}$ cm^{-3}. The OP model is at 152 eV, 1.0×10^{22} cm^{-3} (see End Matter). Model wavelengths are adjusted to align with experiment wavelengths of strong features (Oxygen Ly α, β, γ). Data are excluded at wavelengths with contaminant lines and in Ly α and Ly β saturated line cores. Panel (a) is the 7–14 Å region, primarily bound-free absorption (log scale to facilitate viewing large dynamic range). Panel (b) includes the H-like photon ionization threshold and Ly δ region. Panels (c) and (d) show the Ly γ and Ly β lines, respectively. Panel (e) plots the He β, Ly α, and He-like satellites to Ly α.

The percent difference [defined as 100%* (model–data)/data] between model predictions and measurements of the bound-free opacity ranges from −8.9% [OP] to +10.4% [SCO-RCG], where the values represent an average over the 7–14 Å region [Fig. 3(a)]. Averaging over the seven models, predictions for bound-free opacity agree with the data to within about 5%.

The models predict the H-like ionization fraction is 0.35 ± 0.01 [Fig. 5(a)], indicating that the predicted bound free, mostly due to H-like ions, should agree within about ±3%. However, the SCO-RCG bound-free predictions are higher than OP by about 21% (even though the H-like fraction is lower) and there are notable differences among the other models. This implies that predictions for the excited state populations, the photoionization cross section, or other model approximations are different. There are larger differences between model predictions for the He-like fraction [Fig. 5(b)].

Data-model comparisons [Fig. 3(b)] show that the Ly δ line is more prominent in the data than in most models, possibly because the models overpredict the delocalization of the $n = 5$ level into the continuum or overpredict the broadening, or both. Notable exceptions are the OPAS and PrismSPECT models, which agree reasonably well with the data. Furthermore, the models use approximate methods to redistribute absorption involving delocalized high-n levels and those methods apparently overestimate absorption in the vicinity of the ionization threshold. These observations suggest continued scrutiny of model descriptions for high-n spectral lines merging with the continuum.

The impact of continuum lowering was examined using the Stewart-Pyatt [12] and Ecker-Kroll [13] models (Fig. 7). The Ecker-Kroll approximation overpredicts the continuum lowering. That is, the oxygen Ly δ line is completely merged with the continuum, inconsistent with the oxygen data. On the other hand, the Stewart-Pyatt approximation agrees with the data. This is important because using the PrismSPECT Ecker-Kroll approximation for oxygen would reduce the solar mixture Rosseland mean opacity at the CZB by about 5% (compared to using the Hummer-Mihalas, ion sphere, or Stewart-Pyatt approximations; see Ref. [10]).

The Ly δ delocalization into the continuum is similar for OP [Fig. 2(b)] and the Ecker-Kroll option within PrismSPECT or SCRAM (Fig. 7). This suggests that OP may also overpredict the continuum lowering. Several other models also underpredict the Ly δ [Figs. 6(a), 6(c)] and therefore may overpredict continuum lowering, although by a smaller amount. These findings merit further investigation. Employing an approximation that reduces continuum lowering may raise the solar mixture Rosseland mean opacity by potentially several percent.

The oxygen Ly α opacity comparisons vary widely [Figs. 2(b), 3(e), and 6]. The OP model overpredicts the Ly α opacity compared to the data and OP Ly α opacity predictions are roughly 1.7x higher than with the OPAS model and nearly 2x higher than TOPAZ. This is surprising, considering that the Ly γ and Ly β predictions from all the models agree with each other and with the data [Figs. 3(c) and 3(d)]. It could arise because models predict different Ly α oscillator strengths, blended satellite lines, or line broadening. This finding requires investigations beyond the scope of this Letter, but it could affect the solar mixture Rosseland mean if the discrepancies exist (or are amplified) at CZB conditions [see Fig. 1(c)].

Satellites to Ly α are clearly present in the data [Figs. 2(b), 3(e), and 6]. Predictions from ATOMIC and SCO-RCG agree with the data the best [Figs. 6(a) and 6(d)]. The other models tend to overpredict the satellite opacity [Figs. 6(b), 6(c), 6(e), and 6(f)], except for OP (where the satellites appear to be absent [Fig. 2(b)]). Rosseland mean opacity comparisons between OP and the other models confirm that including the Ly α satellites notably alters the solar opacity.

The overarching picture is that oxygen opacity predictions and measurements agree very well at the n_e and T_e values considered here. However, there are measurable and potentially important differences. Solar Rosseland mean opacity evaluations at the CZB conditions using the seven oxygen models results in differences that range from $+1\%$ (ATOMIC) to -3% (SCRAM), where OP opacities were used for all elements except oxygen and the abundances were from Ref. [17]. The present results suggest that the smallness of these differences may be due to fortuitous canceling errors. For example, OP predicts smaller bound-free opacity than SCO-RCG (Fig. 5), but the OP opacity in the bound-bound region is larger. Thus, the fact that the two oxygen models result in solar Rosseland mean opacities that are only different by about 1% may be partly coincidence. Resolving the solar problem will require careful assessment of model approximations that affect both the bound-bound and bound-free features, since mean opacity deviations larger than 1% are believed important [2–4].

The results presented here provide a foundation for resolving the solar problem in three ways. First, the excellent quantitative agreement between the data and seven opacity models for the bound-free and Ly γ bound-bound line demonstrates that critically important ionization balance predictions are accurate, though this is limited to the explored temperature and density conditions. Discrepancies reported in prior iron opacity research [19–21] highlight the need for oxygen data at higher temperature and density. Nevertheless, it is reassuring that models agree so well with these first-of-a-kind HED opacity measurements. Second, discrepancies between data and models (and between different models) of absorption near the H-like ionization threshold, the Ly α bound-bound line, and satellites to the Ly α line lend immediate motivation for model refinement studies. In fact, some models have already benefited from refinements following their initial comparisons with the data. Finally, the overall agreement supports the accuracy of the experimental methods, including areal density determination, transmission-opacity measurements, and plasma conditions. This fosters confidence in these methods for future solar oxygen opacity measurements at even higher temperature and density.

Acknowledgments—We thank the entire Z facility team and B. M. Jones, and G. A. Rochau for management and encouragement. The authors also acknowledge valuable discussions of the OP opacity model with Professor A. Pradhan (The Ohio State University) and Dr. F. Delahaye (University of Paris–Paris Observatory). Experimental time on the Z facility was provided through the Z Fundamental Science Program. Sandia National Laboratories is a multimission laboratory managed and operated by National Technology and Engineering Solutions of Sandia, LLC, a wholly owned subsidiary of Honeywell International Inc., for the U.S. Department of Energy's National Nuclear Security Administration under Contract No. DE-NA0003525. Los Alamos National Laboratory is operated by Triad National Security, LLC, for the National Nuclear Security Administration of U.S. Department of Energy (Contract No. 89233218CNA000001). Part of this work was performed under the auspices of the U.S. Department of Energy by Lawrence Livermore National Laboratory under Contract No. DE-AC52-07NA27344. This work was supported in part by the Wooton Center for Astrophysical Plasma Properties, NNSA Stewardship Sciences Academic Alliance Award No. DE-NA0004149. T. A. G. acknowledges support from the George Ellery Hale Post-Doctoral Fellowship at the University of Colorado.

This Letter describes objective technical results and analysis. Any subjective views or opinions that might be expressed in the Letter do not necessarily represent the views of the U.S. Department of Energy or the United States Government.

Data availability—The data that support the findings of this article are not publicly available upon publication because it is not technically feasible and/or the cost of preparing, depositing, and hosting the data would be prohibitive within the terms of this research project. The data are available from the authors upon reasonable request.

[1] M. Asplund, N. Grevesse, A. J. Sauval, C. Allende Prieto, and D. Kiselman, Astrophys. J. **417**, 751 (2004).
[2] J. N. Bahcall, A. M. Serenelli, and M. Pinsonneault, Astrophys. J. **614**, 464 (2004).
[3] S. Basu and H. M. Antia, Phys. Rep. **457**, 217 (2008).
[4] G. Buldgen, J.-C. Pain, Philippe Cossé, C. Blancard *et al.*, Nat. Commun. **16**, 693 (2025).
[5] R. M. More, S. B. Hansen, and T. Nagayama, High Energy Density Phys. **24**, 44 (2017).
[6] M. K. G. Kruse and C. A. Iglesias, High Energy Density Phys. **41**, 100976 (2021).
[7] M. Krief, A. Feigel, and D. Gazit, Astrophys. J. **824**, 98 (2016).
[8] R. A Baggott, S. J. Rose, and S. P. D. Mangles, Phys. Rev. Lett. **125**, 145002 (2020).
[9] J. Zeng, C. Gao, P. Liu, Y. Li *et al.*, Sci. China Phys. Mech. Astron. **65**, 233011 (2022); C. A. Iglesias High Energy Density Phys. **47**, 101043 (2023).
[10] B. J. B. Crowley, High Energy Density Phys. **13**, 84 (2014).
[11] T. Gawne, T. Campbell, A. Forte, P. Hollebon *et al.*, Phys. Rev. E **108**, 035210 (2023).
[12] J. C. Stewart and K. D. Pyatt, Jr, Astrophys. J. **144**, 1203 (1966).
[13] G. Ecker and W. Kröll, Phys. Fluids **6**, 62 (1963).
[14] M. J. Seaton, Y. Yu, D. Mihalas, and A. K. Pradhan, Mon. Not. R. Astron. Soc. **266**, 805 (1994).
[15] N. R. Badnell, M. A. Bautista, K. Butler, F. Delahaye, C. Mendoza, P. Palmeri, C. J. Zeippen, and M. J. Seaton, Mon. Not. R. Astron. Soc. **360**, 458 (2005).
[16] C. Mendoza, M. J. Seaton, P. Buerger, A. Bellorin *et al.*, Mon. Not. R. Astron. Soc. **378**, 1031 (2007).
[17] M. Asplund, N. Grevesse, J. Sauval, and P. Scott, Annu. Rev. Astron. Astrophys. **47**, 481 (2009).
[18] S. Rosseland, Mon. Not. R. Astron. Soc. **84**, 525 (1924).
[19] J. E. Bailey, T. Nagayama, G. P. Loisel, G. A. Rochau *et al.*, Nature (London) **517**, 56 (2015).
[20] J. E. Bailey, G. A. Rochau, C. A. Iglesias, and J. Abdallah, Jr. *et al.*, Phys. Rev. Lett. **99**, 265002 (2007).
[21] T. Nagayama, J. E. Bailey, G. P. Loisel, G. S. Dunham, G. A. Rochau *et al.*, Phys. Rev. Lett. **122**, 235001 (2019).
[22] C. A. Iglesias and Rogers, Astrophys. J. **371**, 408 (1991).
[23] T. S. Perry *et al.*, Phys. Rev. E **54**, 5617 (1996).
[24] J. E. Bailey, G. A. Rochau, R. C. Mancini, C. A. Iglesias, J. J. MacFarlane, I. E. Golovkin, C. Blancard, P. Cosse, and G. Faussurier, Phys. Plasmas **16**, 058101 (2009).
[25] D. C. Mayes, B. A. Hobbs, R. F. Heeter, T. S. Perry *et al.*, High Energy Density Phys. **55**, 101177 (2025).
[26] J. E. Bailey, G. A. Chandler, R. C. Mancini, S. A. Slutz *et al.*, Phys. Plasmas **13**, 056301 (2006).
[27] G. P. Loisel, J. E. Bailey, T. Nagayama, S. B. Hansen *et al.*, Phys. Rev. Lett. **134**, 095101 (2025).
[28] T. Nagayama, J. E. Bailey, G. Loisel, G. A. Rochau, J. J. MacFarlane, and I. Golovkin, Phys. Rev. E **93**, 023202 (2016).
[29] T. Nagayama, J. E. Bailey, G. P. Loisel, G. A. Rochau, J. J. MacFarlane, and I. E. Golovkin, Phys. Rev. E **95**, 063206 (2017).
[30] See Supplemental Material at http://link.aps.org/supplemental/10.1103/n2k6-358d, whichprovides a brief description of experimental methods.
[31] H. H. Huang, K. Sequoia, M. Yamaguchi, K. J. Boehm *et al.*, J. Phys. B **54**, 115003 (2021).
[32] T. Nagayama, J. E. Bailey, D. C. Mayes, G. P. Loisel, G. S. Dunham, and T. A. Gomez, Rev. Sci. Instrum. **96**, 033511 (2025).
[33] G. Dunham, T. Nagayama, J. Bailey, and G. Loisel, Rev. Sci. Instrum. **92**, 08351 (2021).
[34] T. Nagayama, J. E. Bailey, G. A. Rochau, S. B. Hansen, R. C. Mancini, J. J. MacFarlane, and I. Golovkin, Rev. Sci. Instrum. **83**, 10E128 (2012).
[35] T. Nagayama, J. E. Bailey, G. P. Loisel, S. B. Hansen, G. A. Rochau, R. C. Mancini, J. J. MacFarlane, and I. Golovkin, Phys. Plasmas **21**, 056502 (2014).
[36] J. Colgan, D. P. Kilcrease, N. H. Magee, M. E. Sherrill, J. Abdallah, Jr., P. Hakel, C. J. Fontes, J. A. Guzik, and K. A. Mussack, Astrophys. J. **817**, 116 (2016).
[37] C. Blancard, P. Cossé, and G. Faussurier, Astrophys. J. **745**, 10 (2012).
[38] C. A. Iglesias, M. H. Chen, V. Sonnad, and B. G. Wilson, J. Quant. Spectrosc. Radiat. Transfer **81**, 227-236 (2003).
[39] J.-C. Pain and F. Gilleron, High Energy Density Phys. **15**, 30 (2015).
[40] S. B. Hansen, J. Bauche, C. Bauche-Arnoult, and M. F. Gu, High Energy Density Phys. **3**, 109 (2007).
[41] J. J. MacFarlane, I. E. Golovkin, P. Wang, P. R. Woddruff, and N. A. Pereyra, High Energy Density Phys. **3**, 181 (2007).
[42] A. K. Pradhan, S. N. Nahar, and W. Eissner, J. Phys. B **57**, 125001 (2024).
[43] F. Delahaye, C. P. Balance, R. T. Syth, and N. R. Badnell, Mon. Not. R. Astron. Soc. **508**, 421 (2021).
[44] A. Serenelli, S. Basu, J. W. Ferguson, and M. Asplund, Astrophys. J. **705**, L123 (2009).
[45] C. E. Starrett, C. J. Fontes, H. B. Tran Tan, J. M. Kasper, and J. R. White, Phys. Rev. E **110**, 045208 (2024).
[46] M. F. Gu and P. Beiersdorfer, Phys. Rev. A **101**, 032501 (2020).
[47] T. Nagayama, J. E. Bailey, R. C. Mancini, C. A. Iglesia *et al.*, High Energy Density Phys. **20**, 17 (2016).
[48] T. A. Gomez, T. Nagayama, P. B. Cho, M. C. Zammit *et al.*, Phys. Rev. Lett. **127**, 235001 (2021).
[49] T. S. Perry, R. F. Heeter, Y. P. Opachich, H. M. Johns *et al.*, High Energy Density Phys. **35**, 100728 (2020).

End Matter

Determining the most relevant oxygen spectral features for the solar CZB opacity—The importance of specific oxygen features for the solar Rosseland mean opacity is quantified by calculating [14–17] the percent mean opacity change per unit wavelength [Fig. 1(c)]. This entails dividing the opacity spectrum into 1500 wavelength increments. A composite opacity is constructed using the total solar opacity including

oxygen, for the ith wavelength interval. The opacity outside the ith interval excludes oxygen. A Rosseland mean is computed from this composite and the Rosseland mean without oxygen is subtracted. This difference represents the Rosseland mean increase from oxygen in the ith interval. The difference, divided by the product of the Rosseland mean without oxygen and the interval width, determines the percent change. Repeating the procedure for every wavelength interval provides the percent change as a function of wavelength.

Plasma diagnostics—The Fig. 4 experiment used a $Mg + SiO_2$ sample, while all others in this Letter used SiO_2. Contaminant lines arise from residual F deposited during the reactive ion etching process used in sample fabrication. These F lines from low-density plasma provide additional wavelength fiducials, and their broadening provides a lower bound for the instrument spectral resolution.

The plasma electron temperature, electron density, and areal density were obtained by comparing measured Si spectra with PrismSPECT model [41] predictions using broadening calculations from [46]. Electron density is determined by fitting the He γ, δ, and ε lines. Lines from lower principal quantum number states were excluded due to large optical depth that introduces difficult-to-quantify uncertainties. Areal density is inferred by integrating under the He δ and He εlines. Electron temperature determination used relative absorption from He γ, δ, and ε lines and associated Li-like satellites. The Si Lyα line was excluded because the predicted H-like ground state population is only 0.01% and small deviations from Local Thermodynamic Equilibrium (LTE) could alter the results. The T_e and n_e uncertainties include contributions from background subtraction, noise, and differences in the values obtained from different spectral lines (see Refs. [27,32]), but do not account for possible systematic model inaccuracies. The use of multiple spectral lines helps mitigate this effect. Furthermore, past investigations showed that the primary diagnostic sensitivity arises from the line broadening model [47]. A preliminary comparison of line broadening results from Ref. [46] and the Balrog code [48] indicates these models agree for the Si lines studied here, but a full quantitative assessment of model sensitivities requires future effort.

This analysis assumes that opacity models for the Si K-shell spectral lines are accurate. This is plausible because Si ions are much more tightly bound than oxygen, rendering the Si atomic states more immune to plasma perturbations. As a cross-check, the plasma conditions were inferred [32,41,46,48] from both Si and Mg lines in the single experiment with Mg in the sample. The T_e and n_e values from the two elements agreed within the uncertainties. It may be possible to further evaluate the spectral diagnostic accuracy using nonspectroscopic diagnostics available in NIF opacity experiments [49].

Opacity—The experimental opacity is inferred by taking the natural log of the transmission and dividing by the oxygen areal density. There are several adjustments made to the data from each experiment before taking the weighted average over all experiments: (1) Data points with transmission <0.1 are deleted, to avoid line saturation. (2) The Si L-shell absorption predicted with PrismSPECT [41] at the nominal T_e, n_e conditions is subtracted, after scaling by the oxygen to silicon areal density ratio. The oxygen-equivalent scaled Si L-shell opacity is roughly 100 cm^2/g at the long wavelength end

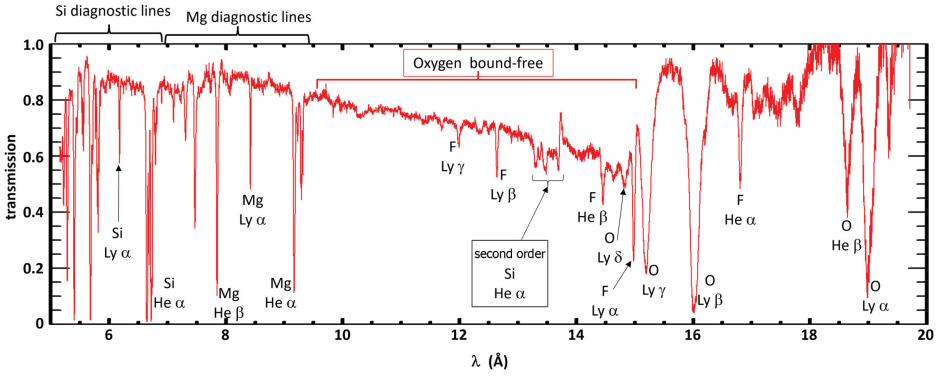


FIG. 4. Transmission averaged over six spectrometers from oxygen experiment z3787 that used 1.9×10^{19} oxygen atoms/cm^2 areal density. The plasma temperature, density, and areal density are inferred from the Si and Mg bound-bound lines. Fluorine lines arising from contamination during fabrication serve as wavelength fiducials and instrument resolution constraints, but do not affect transmission because they occur in both the attenuated and unattenuated signals and the F areal density is low. The second order Si Heα contamination is an artifact. Spectra recorded with RAP crystals are not corrected for second order, because the second order RAP reflectivity drops by more than an order of magnitude above the second order Rb edge at 13.65 Å. Spectra from KAP crystals are corrected for second order and averaging KAP and RAP data ameliorates any effect on the final inferred opacity, but the true opacity value between roughly 12.5–13.5 Å may be slightly higher than reported.

of the spectrum, and it shrinks at shorter wavelengths. While small, this contribution is not negligible in the low opacity region between the O Ly β and He β lines. PrismSPECT and ATOMIC [36] Si calculations agree within 5% over the 12–22 Å range, helping evaluate possible model errors. (3) Data points corresponding to diagnostic lines, known contaminant lines, and crystal artifacts are deleted from the oxygen opacity spectra. (4) Oxygen opacity was limited to $\lambda > 7.0$ Å to avoid the forest of Si lines and the need to account for Si bound-free.

The model predictions for the H-like oxygen fraction agree with each other [Fig. 5(a)]. This is notable since the bound-free opacity from 7–14 Å is dominated by H-like ion absorption, yet the bound-free predictions differ. This suggests that model approximations affecting bound-free predictions vary between models. Model predictions for He-like ionization [Fig. 5(b)] differ by about ±20%, warranting future evaluation.

The calculated opacities are converted into "experiment-equivalent opacity," defined as in Ref. [19], before comparing with the data. Each calculated opacity is used to compute transmission based on the experiment areal density. The transmission is convolved with the instrument response and then converted back into opacity. This procedure is repeated for each experiment areal density and the result is averaged, since the weighted average experimental result is from six different experiments. Experiment equivalent opacity comparisons with the seven models are shown in Figs. 2(b) and 6. Examination of the Hummer-Mihalas, Ecker-Kroll, and Stewart Pyatt approximations for continuum lowering [10–13] are shown in Fig. 7.

The model wavelengths were adjusted to match the experimental values using a "block shift" procedure that separately shifts the Ly δ-Ly β region and the He δ-Ly α satellite region, typically by about 10 mÅ and no more than 28 mÅ. This promotes quantitative opacity accuracy assessments but may mask atomic structure errors. The small wavelength differences merit future investigation.

The online OP model [16] used here [Fig. 2(b)] corresponds to $T_e = 152$ eV and $n_e = 1.0 \times 10^{21}$ cm^{-3}, slightly different from the $T_e = 148 \pm 4$ eV and $n_e = 8.6 \pm 1.4 \times 10^{21}$ cm^{-3} experimental values. The OP model conditions are still within the experimental uncertainties. However, to further investigate possible impact, a PrismSPECT [41] calculation was performed at the same conditions as OP. The differences between PrismSPECT opacities at the OP conditions and the nominal conditions was small. This is not surprising, since increasing both T_e and n_e tends to preserve the charge state distribution that helps control the opacity.

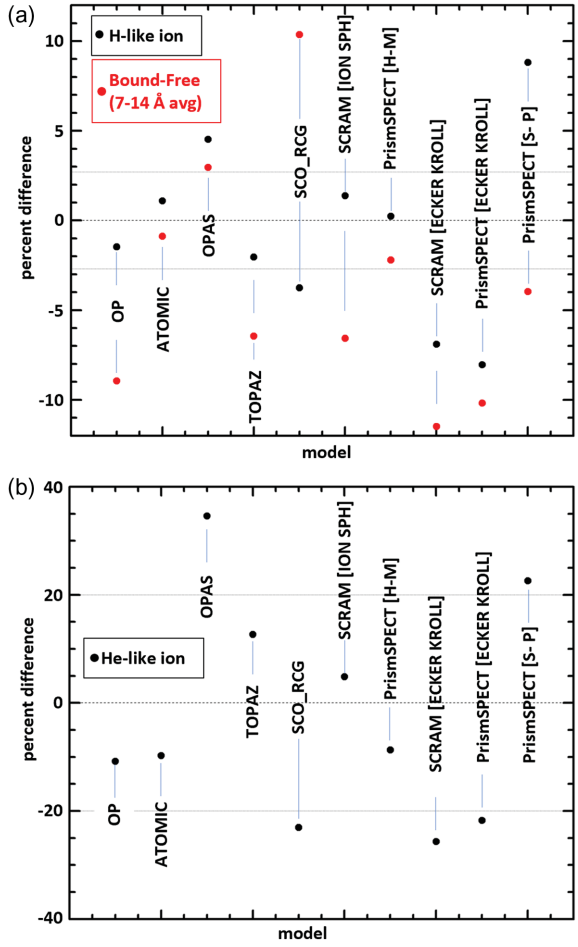


FIG. 5. Model predictions for percent difference H-like (a) and He-like (b) ionization fraction [black dots, defined as (model-average prediction)/average prediction)]. The SCRAM model used the ion sphere and Ecker-Kroll IPD approximations and PrismSPECT used the Hummer-Mihalas (H-M), Ecker-Kroll, and Stewart-Pyatt (S-P) IPD approximations. All other models used their default IPD method. The average H-like and He-like fraction predictions are 0.35 and 0.039, respectively, at the experiment conditions. The bound-free opacity percent difference averaged over 7–14 Å (a), red dots) is defined as (model–data)/data.

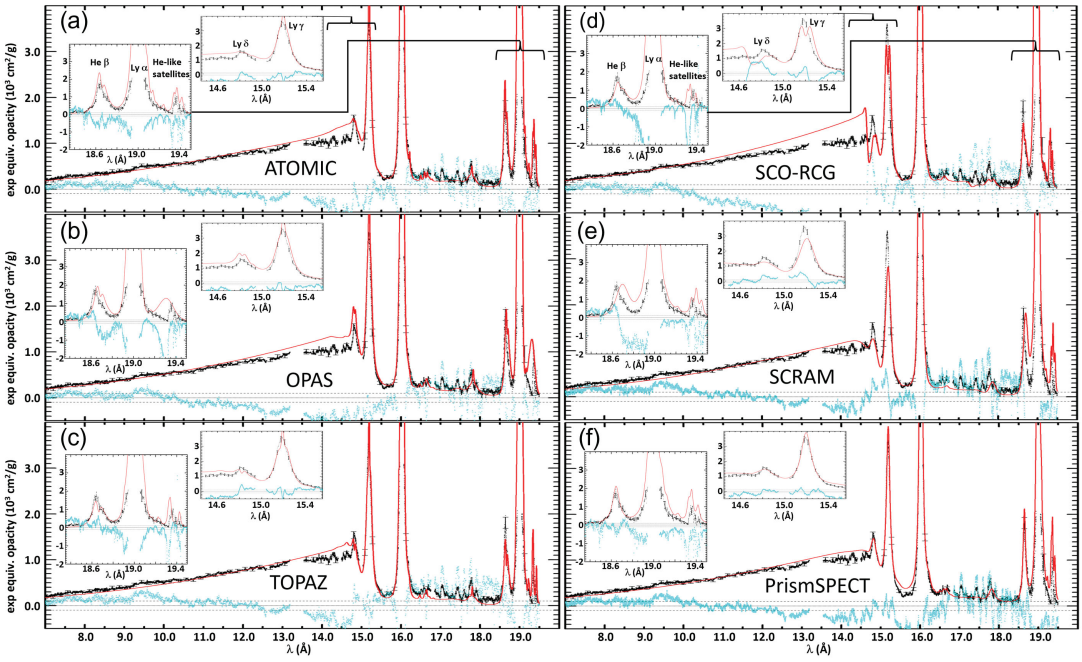


FIG. 6. Oxygen weighted average opacity from six Z experiments (black dots with error bars) compared with opacity model calculations (red) at $T_e = 148$ eV and $n_e = 8.6 \times 10^{21}$ cm^{-3}. The models are ATOMIC (a), OPAS (b), TOPAZ (c), SCO-RCG (d), SCRAM (e), and PrismSPECT (f). The cyan curve is residual = [(data–model)/uncertainty], multiplied by 100 to place it on the same scale as the opacity. The horizontal dash lines represent residual difference $= 1\sigma$. The insets are enlarged views of the oxygen Ly γ-Ly δ and He β-Ly α-He–like satellite regions.

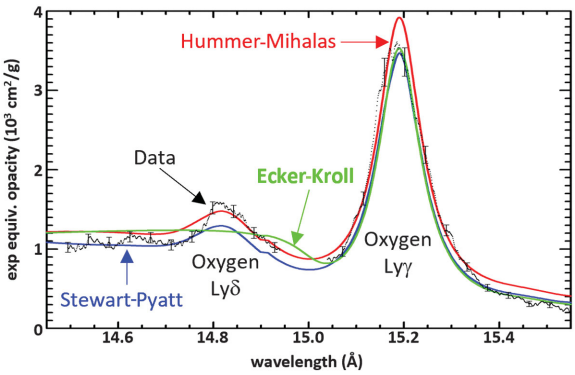


FIG. 7. Oxygen opacity data (black dots, 1σ error bars) compared to PrismSPECT predictions using Hummer-Mihalas (red), Ecker-Kroll (green), and Stewart-Pyatt (blue) approximations for continuum lowering [see Refs. [10–13]].